PHILOSOPHICAL TRANSACTIONS OF THE ROYAL SOCIETY A MATHEMATICAL, PHYSICAL & ENGINEERING SCIENCES

Nanotips and Nanosources: Application to Low-Energy-Electron Microscopy

Vu Thien Binh, N. Garcia and V. Semet

Phil. Trans. R. Soc. Lond. A 1995 **353**, 281-290
doi: 10.1098/rsta.1995.0100

Nanotips and nanosources: application to low-energy-electron microscopy

By Vu Thien Binh[1], N. Garcia[2] and V. Semet[1]

[1]*Département de Physique des Matériaux, UA CNRS Université Claude Bernard, Lyon 1, 69622, Villeurbanne, France*

[2]*Fisica de Sistemas Pequenos, CSIC Universidad Autonoma de Madrid, CIII, 28049 Madrid, Spain*

The characteristics of e-beams field emitted from nanotips, which are atom-sources of electrons, were analysed experimentally for non-magnetic and ferromagnetic nanotips. Their specific characteristics are fully exploited in a versatile low-energy electron projection microscope: the Fresnel projection microscope. Observations of nanometric fibres of carbon and of organic materials were performed with working voltages around 200 V. The images show, in the direct space, details of the objects of less than 1 nm without any magnetic shielding.

1. Introduction

In the history of electron optics and electron microscopy, a major instrumental development occurred in the early 1960s when field-emission guns (FEG) replaced thermionic devices. In 1965, Crewe became the first to experimentally demonstrate the dramatic improvement in the resolution of scanning electron microscopy by using a field emission (FE) tip as an electron source, in which the electron beam can be focused onto a probe area of only a few ångströms in diameter (Crewe 1965; Crewe *et al.* 1968).

Further progress in FEGs can be made if new improvements to the FE tip can be realized: in particular, decreasing the size of the field emitting area to increase the stability of the emission and to narrow the energy spread of the FE electrons. We review in this paper some of the main experimental characteristics—confinement of the emitting area, stability, energy spread, etc.—obtained with field emission from nanotips. These specific behaviours were observed with nanotips, which consist of single-atom sharpness nanoprotrusions, 2–5 nm in height, on top of hemispherical base-tips, and for which the whole FE current is emitted from the topmost apex atom (Binh 1988; Binh & Garcia 1991). The particular electron and ion beam patterns emitted from ferromagnetic nanotips will also be described and discussed.

We take advantage of the unique FE properties of the nanotips to further the limits of electron microscopy with a very versatile low-energy-electron projection microscope, based on the nanotip as a nanosource. This compact microscope has been used for observations of polymers with nanometric resolution.

Phil. Trans. R. Soc. Lond. A (1995) **353**, 281–290
Printed in Great Britain

2. Nanotips

(a) Confinement of the field emitting area

The FE area, namely the emitting zone at the tip apex concerned, is governed principally by the tip geometry and, in particular, by the apex structure. Three processes can be used for narrowing the FE area at the apex: (i) decreasing the whole tip radius, i.e. to produce ultra-sharp hemispherical tips (Muller 1937; Janssen & Jones 1971); (ii) confining the emission over a small area by modifying the atomic structure and/or the work function in the apex region of hemispherical tips, namely build-up tips (Sokolovskaia 1956; Bettler & Charbonnier 1960; Swanson & Crouser 1969; Veneklaasen & Siegel 1972); and (iii) confining the field over the apex of a protruding zone, i.e. to fabricate on top of the hemispherical base tip a nanoscale protrusion tip, named the nanotip or teton-tip (Binh 1988; Binh & Garcia 1991).

A comparative study of the above tips and three-dimensional atomic-scale calculations of the distribution of the field at the apex zone (Atlan *et al.* 1992) showed a field enhancement factor in the range of 7–10 at the nanotip apex compared to the surrounding area of the substrate tip. This field confinement means that all of the FE current comes exclusively from the single-atom apex. No other FE pattern out of this spot is observed over the entire range of applied voltage V_{App} for field emission observation of the nanotips without its destruction. This unique behaviour is not observed for ultra-sharp and build-up tips.

(b) Fashioning nanotips (Binh 1988; Binh & Garcia 1991)

(i) *Growth of nanoprotrusions*

By the application of a high field, and at a temperature of around a third of the bulk melting temperature of a metal, a two-dimensional melting layer is created which facilitates an increase of the height of some existing protrusions due to the field gradient driving force over the thermally induced corrugations leading to the formation of nanoprotrusions. The geometry of the nanoprotrusions formed is then determined by the equilibrium between the pulling-out of the electric field gradient force and its blunting due to the capillary force. A schematic drawing of this mechanism is given in figure 1. For a certain critical height, the field at the apex of the protrusion is high enough to field evaporate the topmost atom leading then to the generation of a stable atomic metallic ion emission (AMIE) beam of 10^5–10^6 ions s^{-1} of the tip metal itself.

(ii) *Fashioning nanotips*

By fast cooling of this protrusion it is possible to freeze its geometry, which appears to be a ⟨111⟩-pyramid with dimensions in the range 2–3 nm (for the base and the height) ending in one atom. These nanoprotrusions sit on the top of the macroscopic tips and are teton-tips or nanotips (Binh 1988; Binh & Garcia 1991).

3. Specific field emission properties of the nanotips

The field electron emission properties of the nanotips have been characterized. The results show unique properties that are attributed to the atomic scale of the emission area. The results are as follows.

(i) The FE current comes exclusively from the single-atom apex.

(ii) The e-beam is autocollimated to 4–6°.

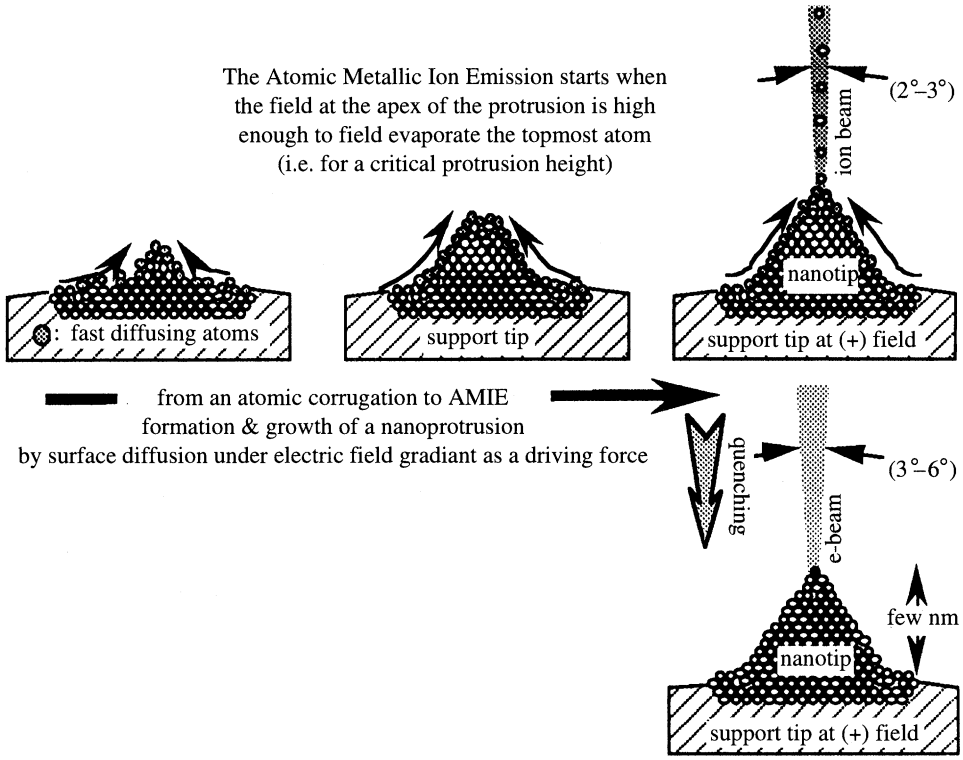

Figure 1. Schematic drawing of the formation of a nanotip under temperature and field. The nanotip can be either a nanosource of metallic ions or of electrons by changing the polarity.

(iii) The emitted electrons do not present a continuous energy distribution up to the Fermi level; they come exclusively from localized energy bands. This behaviour is reflected by the presence of individual peaks in the total energy distribution (TED) spectra when the protrusion height is important enough (Binh *et al.* 1992*a*, 1993). This means that the energy distribution of the electron beam, without any energy filter, could be as small as 0.1 eV at room temperature or 0.07 eV at *ca.* 77 K (Purcell *et al.* 1995).

(iv) The I–V characteristics no longer follow the Fowler–Nordheim law; they show a characteristic saturation of the current versus V_{App}.

(v) The FE current is very stable; variation of less than 1% was observed for a period of 10 h for current values $\leqslant 1$ nA.

(vi) For higher currents, up to 0.1 μA, there exist reversible jumps of the current between two discrete values (or even more for the highest currents), which is termed 'flip-flop'. These reversible and discrete jumps in the FE current are induced by atomic movements between two neighbouring states of the geometry at the apex, which leads to changes in the local field distribution and in the TED of the emitting electrons (Binh *et al.* 1992*b*).

The nanotips are then atomic-size sources of electrons, giving monochromatic and coherent beams with high stability and exceptional brightness (10^6–10^8 A cm^{-2} str^{-1} at *ca.* 100 V).

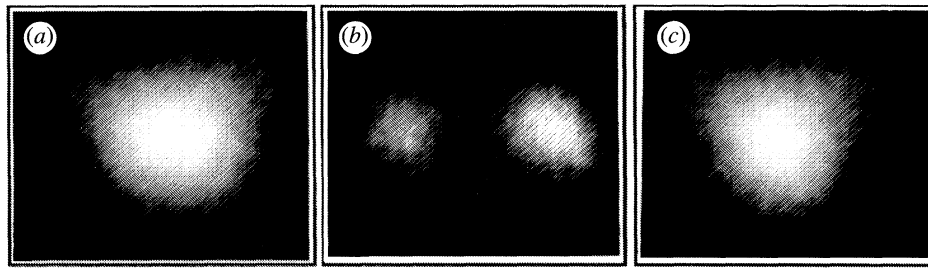

Figure 2. Sequence of a splitting process followed by the merging of the two e-beams coming from a Fe nanotip when the tip temperature T crosses the Curie point T_C: (*a*) $T \approx 1100$ K $> T_C$; (*b*) $T \approx 77$ K $< T_C$; (*c*) $T \approx 1100$ K $> T_C$.

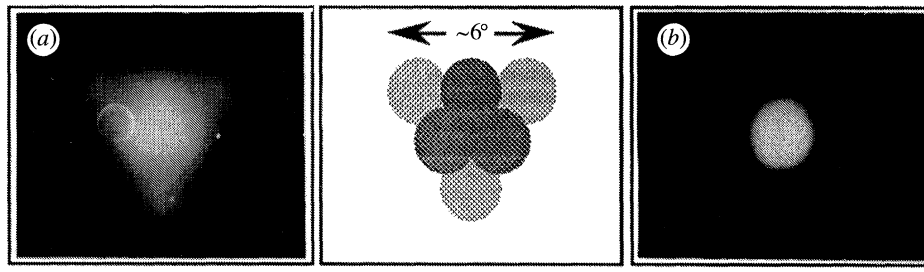

Figure 3. Comparison between (*a*) typical Fe-AMIE pattern, with a sextuplet spot pattern, and (*b*) Au-AMIE pattern, which is only a spot.

4. Specific field emission properties of the ferromagnetic nanotips (Binh & Garcia 1994)

(*a*) *Electron beams*

The Fe nanotips presented most of the FE characteristics found for non-magnetic nanotips described above. To assess the influence of the magnetism, we have studied the field electron emission from these ferromagnetic nanosources as a function of the temperature and, in particular, its behaviour when the temperature crosses the bulk Curie temperature T_C (1042 K). The observed field emission microscopy (FEM) patterns are presented in figure 2. The V_{App} in this example is *ca.* 2870 V. The experimental procedure was as follows. A stable single spot pattern coming from a nanoscale protrusion was obtained at *ca.* 1100 K. The heating current was then cut, leading to the cooling of the tip to liquid nitrogen temperature while the FEM patterns were recorded on video. The sequence shows mainly that the splitting or merging of the electron beam(s) occurs when the nanotip temperature crosses a critical temperature, which is near the Curie temperature, and that it is a reversible process. The splitting angle of the doublet depends on the temperature of the nanotip, with a maximum in the range of 4–6°.

It is important to note that none of these observations took place for W and Au nanotips or for standard magnetic Fe microtips. In this last case, this may be because the splitting of the beam occurs only for the atomic scale geometry of the magnetic protrusion, or its observation is masked by the spatial resolution limit of the magnetic microtips and their beam opening is *ca.* 90° while the splitting is 6°.

(*b*) *Ion beams*

There are also effects on the AMIE beams unique to the magnetic nanotips which could have the same physical cause as for the electron beams. AMIE was observed for temperatures between 600 and 800 K and for V_{App} between +5.5 and +11 kV which corresponds to an electric field range of 18–24 V nm^{-1}. These values were estimated from the ionization field of 35 V nm^{-1} for Ne (Atlan *et al.* 1992) and the voltages needed for field ion microscopy (FIM) observations of the topmost atom of the protrusions with Ne as the imaging gas. The temperature range to achieve AMIE is around one third of the bulk melting temperature and is below T_C. In other words, AMIE could not be achieved above T_C. This temperature range for AMIE, compared to the bulk melting point, is similar to the temperature range needed for AMIE of W, Pt or Au.

The big difference with W, Pt or Au are the particular patterns of the Fe AMIE spots (figure 3). Figure 3*a* shows specific Fe AMIE patterns. A characteristic pattern is a triangular sextuplet spot shape with sharp edges. The opening angle between two extremities of the triangle is *ca.* 6°, and between each spot it is *ca.* 2°. The intensity of the triplet inside is higher than for the triplet at the outskirts. In order to compare AMIE patterns between Fe and non-magnetic tips, we present in figure 3*b* a typical spot of AMIE from Au tips. For non-magnetic nanotips, such as W, Pt and Au, only a single spot with an opening angle of 2–4° was observed for the whole AMIE temperature range (Binh 1988; Binh & Garcia 1991).

(*c*) *Discussions*

To explain these data, we have envisaged two general mechanisms based on the magnetic phase transition.

1. Geometrical interpretation. The splitting of the e-beam is due to the reversible formation of two protrusions during the magnetic phase transition and AMIE multiplet-spots are emitted from an aggregate of protrusions. The aggregation or splitting of the protrusions are due to a rearrangement of the structure caused by magnetic interaction for temperatures under T_C. We find this hypothesis difficult to handle in view of the weak magnetic energy (order of meV) versus the structure modification energy (order of eV). Furthermore, the observed conservation of the AMIE sextuplet patterns during their movement and also during their partial overlapping would not occur in the case of aggregates of protrusions. Also, the observed patterns and their symmetries are different for FE and AMIE.

2. Magnetic interpretation. First of all, our calculations show that classical explanations taking into account the deviation of the emitted beams by the magnetic field of the bulk tip can be ruled out. The beam deviations in that case are orders of magnitude too small and also cannot produce the observed patterns. This leads to the conclusion that the effect must be due to a very strong magnetic interaction at the atomic scale. This could be either a scattering process, a magnetic diffraction (Aharonov–Bohm-like) (Olaru & Popescu 1985), Stern–Gerlach-like spin selection (Mott & Massey 1976; Kessler 1976) or Lorentz-force beam deviations under very large and localized magnetic gradient existing at the apex of the ferromagnetic nanotips. The different patterns observed reflect the magnetic state of the different particles (ions or electrons), the three-dimensional field distribution at the atomic scale apex region and the nature of the interaction.

PHILOSOPHICAL TRANSACTIONS OF THE ROYAL SOCIETY A MATHEMATICAL, PHYSICAL & ENGINEERING SCIENCES

At present we cannot assess which of these mechanisms, alone or in concomitance, is the proper one for explaining the presented phenomena. We can, however, state that Fe nanotips present specific magnetic properties attached to the atomic size of these nanosources.

5. Low-energy-electron projection microscope: observations of nanometric carbon fibres (Binh *et al.* 1994)

We now take advantage of the unique FE properties of the nanotips and use them in a projection microscope. Projection microscopy was first proposed by Morton & Ramberg (1939) with their point projector electron microscope. Based on the same principle, Muller (1968) and Muller & Tsong (1969) later introduced the field-ion shadow projection microscope. The potential of the projection microscope for electron microscopy was already perceived by Morton & Ramberg (1939). In the projection or shadow microscope (figure 4*a*), the greatly magnified shadow of an object can be obtained by making use of the quasi-radial propagation of field emitted electrons, or ions coming from a tip, when the object is inside the beam path. This 'involves no electron-optical lens elements, the images obtained are free from the ordinary aberrations. The limit of resolution depends solely on the distribution of initial velocities of the field electrons and on Fresnel diffraction by the object'. By using the projection law, the image has a magnification factor M given by $M = i/o \approx D/d$; where i and o are the image and object dimensions and D and d are the distances of the tip to the screen and to the object, respectively. This equation shows that the magnification increases by approaching the object to the tip and that it could reach values in the range of 10^7–10^6 for tip–object distances of between 10–100 nm, with the screen located 10 cm away from the tip.

However, the lack of good mechanical stability and adequate controlled nanoscale approach devices has limited the magnification of the projection microscope to *ca.* 3000× for the first realization (Morton & Ramberg 1939), then up to *ca.* 20 000× with a resolution of about 50 nm in later attempts (Melmed 1968; Piquet *et al.* 1970). With the recent technological developments of scanning tunnelling microscopy, tip–sample distances of less than 1 nm can now be routinely handled by using piezodrives (Chen 1993) for nanometric displacements. Recently, it has become possible to observe diffraction patterns by carbon fibres, with diameters between 10–20 nm, with magnifications of the order of 10^5–10^6 (Fink *et al.* 1990; Spence *et al.* 1993).

(*a*) *Experimental set-up*

In our projection microscope, the nanosources were W nanotips. They were fashioned *in situ* by the AMIE technique using a W-⟨111⟩ single crystal as a base tip. The nanosources give a spot of less than 1 cm diameter on the observation screen that is placed 10 cm from the tip. With an applied field emission voltage in the range of 50–300 V, depending on the tip–object distance, the current of each spot was in the range of 10^{-12}–10^{-11} A. The stability of the FE of the nanotips in the projection mode is typically *ca.* 5 h, with an upper limit of *ca.* 10 h and a minimum of 2–3 h.

The absolute dimensions of the samples and the x–y scales given in our figures were measured directly by following the displacement of the projection images on the screen against the motion of the object under controlled deflections of the sample-holder piezotube. The x–y dimensions of the object are then determined directly

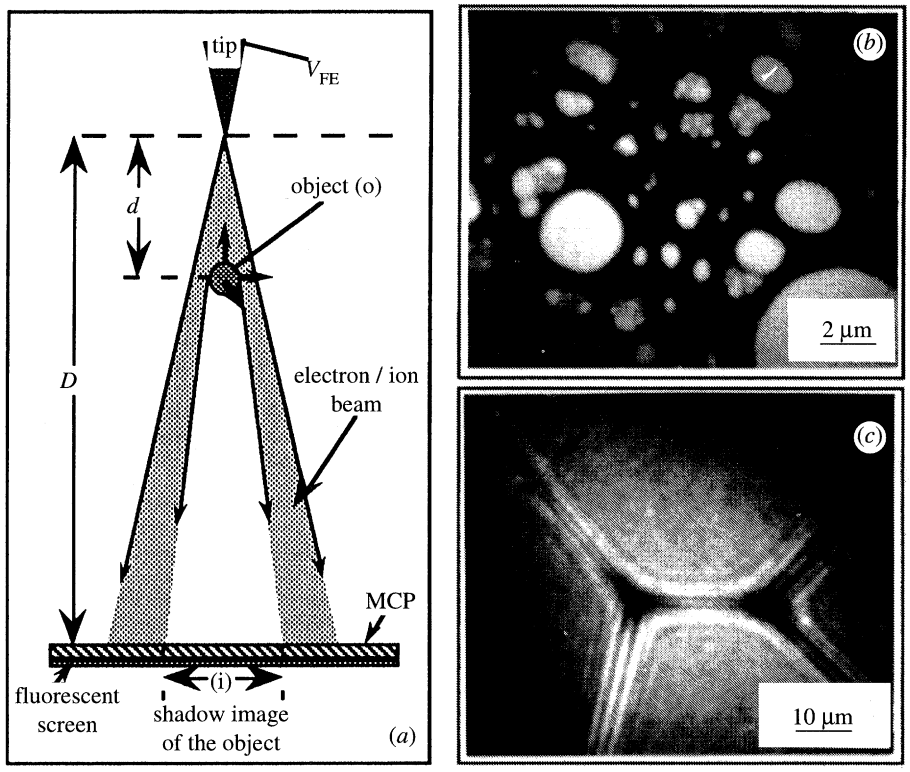

Figure 4. (*a*) Schematic drawing of a projection microscope; (*b*) shadow image of carbon holes at low magnification (380 V); (*c*) Fresnel diffraction by carbon fibres (290 V). The arrow shows a nanometric defect on the fibre.

for any nanotip–object distances with an accuracy given by the piezodrives, the behaviours of which are now very well known (Chen 1993).

(*b*) *Observations of carbon fibres*

The observed samples were commercial carbon holey films deposited on 3 mm transmission electron microscopy (TEM) gold grids. The sample structure allows not only the observations of holes but also of carbon fibres in the range from μm down to few nm.

At large tip–object distances, the images of a micrometre-scale hole of the carbon membrane show one bright line along their edge (figure 4*b*). Observation of resolved interference fringe patterns is possible when the tip–object distances become small enough, i.e. when there is enough magnification to separate the fringes. Figure 4*c* is a characteristic image obtained with fibres of the holey carbon film. These projection images were direct photographs of what can be seen on the screen without any image treatment. The sharpness of the fringes covering the whole beam area, reflects the very high degree of coherence of the electron beam coming from the nanotip. Furthermore, direct observations of nanometric structural features can be achieved, as is shown by the measurable bending of the carbon fibres near the defect zones of partial cutting of the fibre in figure 4*c*.

(c) Discussions

(i) Our experimental results show interference patterns that are very well explained by Fresnel diffraction by a small wire, as was originally predicted (Morton & Ramberg 1939).

(ii) The fringes were present over the whole beam area, showing its very high degree of coherence, as was predicted for single atom sources (Garcia & Rohrer 1989).

(iii) The experimental results presented in this paper have been achieved without any magnetic field shielding. The sharp diffraction figures obtained are experimental proof that a projection microscope using a nanotip as a coherent nanosource does not need magnetic protection in order to perform Fresnel diffraction. This has to be related to the protruding geometry of the nanotips and the atomic size of the FE area, namely the sub-atomic dimension of the virtual source. Under our experimental conditions, simple calculations (Feynmann *et al.* 1964) of the deviations of the image at the screen by Aharonov–Bohm and Lorentz-force effects due to the stray fields give deviations that are orders of magnitude smaller than the fringe widths at the screen. Thus, the blurring will not prevent the observation of the interference fringes.

6. Low-energy-electron projection microscope: observations of polymers with nanometric resolution (Binh *et al.* 1995)

In view of the above results, the projection microscope operating with nanotips is a very versatile instrument for observing nanoscale objects and performing diffraction patterns at energies of hundreds of volts, i.e. a proper tool for observations of small organic materials and macromolecules. 'This brings us to another motivation, namely to work with selected individual macromolecules. Of great interest to macromolecule chemistry and biology itself, this capability will be a crucial element for the building and control of molecular assemblies.' (Rohrer 1991).

(a) Sample preparation

The polymers we have observed are hollow macroscopic fibres used in the fabrication of dialysis filters. The polymers are a mixing of polysulfone-bis-phenol-A (95%) and polyvinyl-pyrrolidone (5%). The hollow fibres were dissolved in chloroform to a concentration of 5.25 mg l^{-1} (the polymer and its dissolution has been prepared by R. Semet and Pham Quang Tho of the Service Central d'Analyse-CNRS Solaize) in order to separate them into polymer chains. The projection sample is then prepared by putting one drop of this solution over the holey carbon grid. After the evaporation of the solvent, the probability of having polymers stretching across a hole is important, as shown in figure 5*a*.

(b) Experimental results and discussions

Figure 5 shows a polymer net at different magnifications. The main results are as follows.

(i) Polymers can be observed with a projection microscope using nanotips as a point source. They are arranged into a polyhedric net with fibres of different lengths and different diameters down to few nanometers.

(ii) Nanometric resolution can be achieved with an e-beam energy in the range of 200–300 eV without any observable degradation of the sample under the beam, even after observations lasting 1 h. This is in agreement with our estimation of the radiation damage by the electron irradiation.

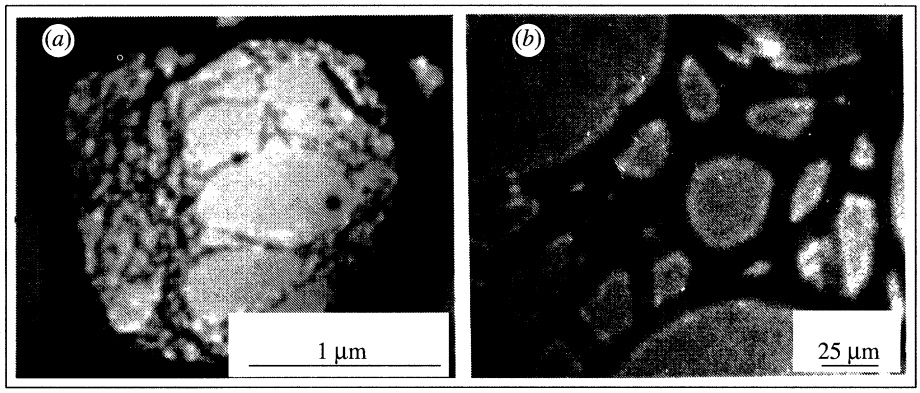

Figure 5. Projection microscopy images of polymers stretching across a carbon hole: (*a*) 720 V; (*b*) 270 V.

(iii) Compared to carbon fibres of the same dimension, the polymer images are less sharp, even when the fringes are well resolved.

(iv) Inside the Fresnel diffraction patterns of the fibres, a periodic variation of intensity with *ca.* 5 nm spacing could be observed, in contrast with carbon fibre observations. This periodic contrast has to be related to the variation of the transmission factor of the polymer nanofibres having the same period. This is probably due to a periodic repetition of some nanometric motif that constitutes the polymer nanofibers.

(v) Using the same sample, we were not able to observe the described polymer structures with a conventional transmission electron microscope.

7. Conclusions

The protruding geometry of the nanotips allows them to be atomic-size nanosources of electrons and ions with unique properties. By the use of these nanotips inside a projection microscope and taking advantage of the fact that they are nanosources of monochromatic and highly coherent electron beams, we have pushed forward the ultimate limits of electron microscopy. It is now possible to observe the individual supramolecular structure of polymers with nanometric resolution with a versatile compact lensless low-energy-electron projection microscope which was discovered more than fifty years ago.

The contribution of Dr R. Semet and Dr Pham Quang Tho, Service Central d'Analyse/Département Instrumentation (CNRS-Solaize), is highly appreciated. We thank S. T. Purcell for his contribution and thorough discussions on all the subjects. This work has been supported by European Community Contracts, by French and Spanish Government Agencies.

References

Atlan, D., Gardet, G., Binh, V. T., Garcia, N. & Saenz, J. J. 1992 *Ultramicroscopy* **42–44**, 154.
Bettler, P. & Charbonnier, C. 1960 *Phys. Rev.* **119**, 85.
Binh, V. T. 1988 *J. Microscopy* **152**, 1355.
Binh, V. T. & Garcia, N. 1991 *J. Phys., Paris* I **1**, 605.
Binh, V. T. & Garcia, N. 1995 *Surf. Sci.* **20**, L69.
Binh, V. T., Semet, V. & Garcia, N. 1994 *Appl. Phys. Lett.* **65**, 2493.

PHILOSOPHICAL TRANSACTIONS OF THE ROYAL SOCIETY A MATHEMATICAL, PHYSICAL & ENGINEERING SCIENCES

Binh, V. T., Semet, V. & Garcia, N. 1995 *Ultramicroscopy* (in the press).

Binh, V. T., Purcell, S. T., Garcia, N. & Doglioni, J. 1992*a* *Phys. Rev. Lett.* **69**, 2527.

Binh, V. T., Purcell, S. T., Gardet, G. & Garcia, N. 1992*b* *Surf. Sci.* **279**, L197.

Binh, V. T., Purcell, S. T. & Garcia, N. 1993 *Phys. Rev. Lett.* **19**, 2504.

Chen, J. C. 1993 *Introduction to scanning tunneling microscopy (Oxford series in optical and imaging sciences)*. New York: Oxford University Press.

Crewe, A. V. 1965 *Conf. on Non-Conventional Electron Microscopy (Cambridge).*

Crewe, A. V., Walls, J. & Welter, L. M. 1968 *J. Appl. Phys.* **39**, 5861.

Feynman, R. P., Leghton, R. B. & Sands, M. 1964 *The Feynman lectures in physics*, vol. II. Reading, MA: Addison-Wesley.

Fink, H. W., Stocker, W. & Schmid, H. 1990 *Phys. Rev. Lett.* **65**, 1204.

Garcia, N. & Rohrer, H. 1989 *J. Phys.: Condens. Matter* **1**, 3737.

Janssen, A. P. & Jones, J. P. 1971 *J. Phys.* D **4**, 118.

Kessler, J 1976 *Polarised electrons* p. 1. Berlin: Springer.

Melmed, A. J. 1968 *Appl. Phys. Lett.* **12**, 100.

Morton, G. A. & Ramberg, E. G. 1939 *Phys. Rev.* **56**, 705.

Mott, N. F., Massey, H. S. W. 1965 *Theory of atomic collisions*, p. 210. Oxford: Clarendon.

Muller, E. W. 1937 *Z. Phys.* **106**, 132.

Muller, E. W. 1968 *15th Field Emission Symposium (Bonn).*

Muller, E. W. & Tsong, T. T. 1969 *Field ion microscopy: principle and applications* p. 129. New York: Elsevier.

Olaru, S. & Iovitzu Popescu, I. 1985 *Rev. Mod. Phys.* **57**, 339.

Piquet, A., Roux, H., Binh, V. T., Uzan, R. & Drechsler, M. 1970 *Rev. Phys. Appl.* **5**, 645.

Purcell, S. T., Binh, V. T. & Garcia, N. 1995 *Appl. Phys. Lett.* **67**, 436.

Rohrer, H. *Highlights in condensed matter physics and future prospects (NATO-ASI Series B: Physics)* (ed. L. Esaki), vol. 285. New York: Plenum.

Sokolovskaia, I. L. 1956 *J. tech. Phys. (URSS)* **26**, 1177.

Spence, J. C. H., Qian, W., Liu, J. & Lo, W. 1993 *Proc. 51st Annual Meeting of the Microscopy Society of America* p. 1060.

Swanson, L. W. & Crouser, L. C. 1969 *J. appl. Phys.* **40**, 4741.

Veneklaasen, L. H. & Siegel, B. M. 1972 *J. appl. Phys.* **43**, 1600.

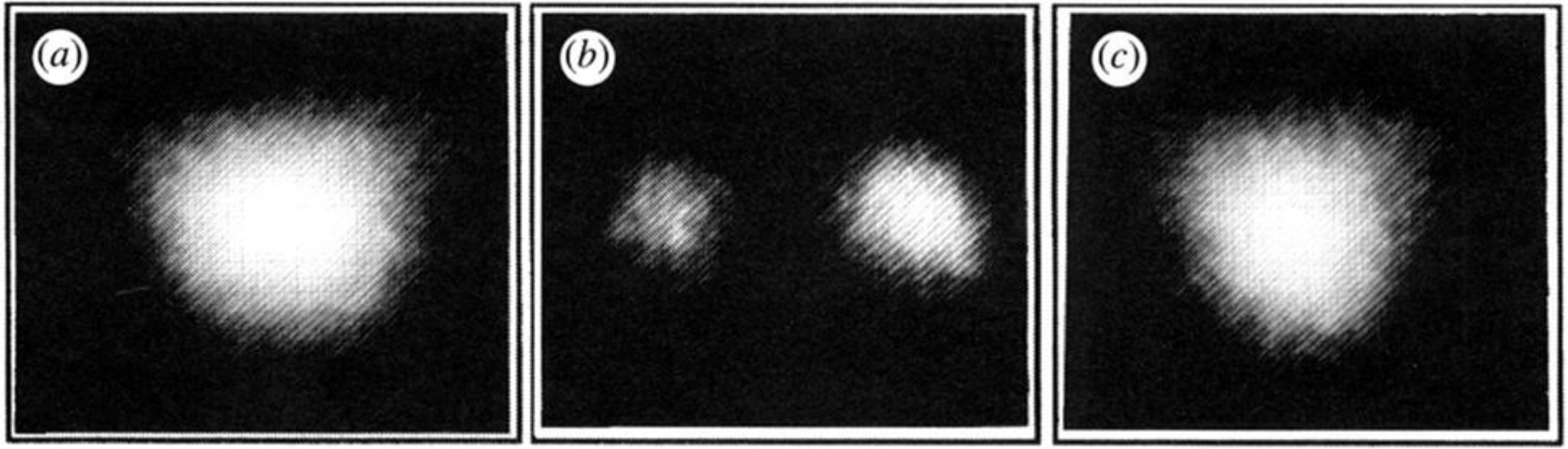

igure 2. Sequence of a splitting process followed by the merging of the two e-beams coming om a Fe nanotip when the tip temperature T crosses the Curie point T_C: (a) $T \approx 1100$ K $> T_C$;) $T \approx 77$ K $< T_C$; (c) $T \approx 1100$ K $> T_C$.

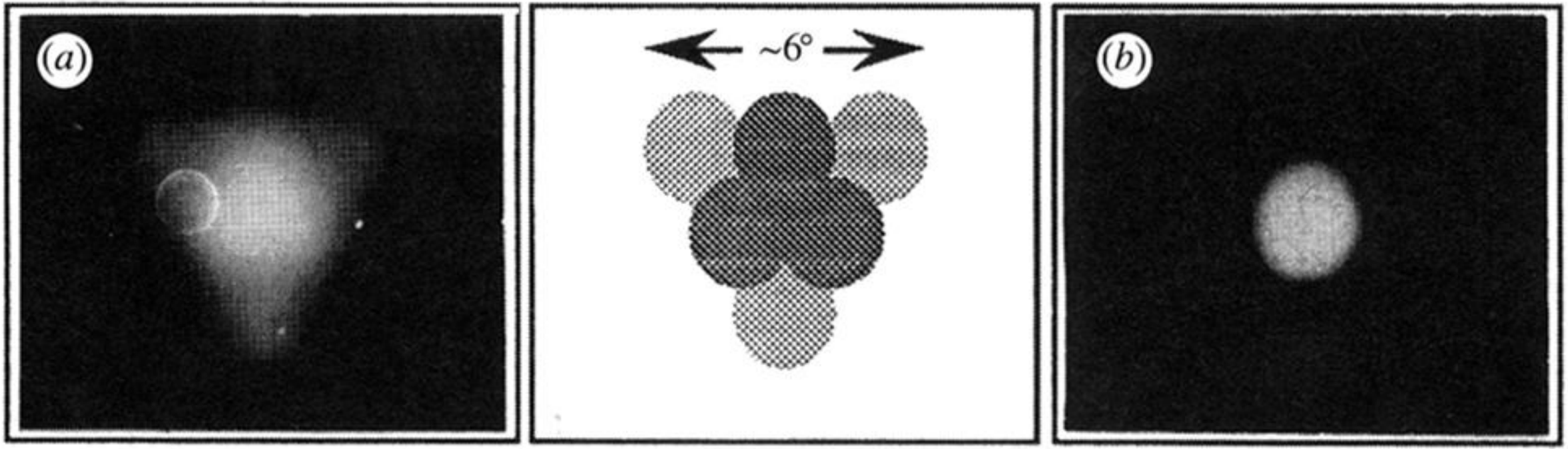

gure 3. Comparison between (*a*) typical Fe-AMIE pattern, with a sextuplet spot pattern, and (*b*) Au-AMIE pattern, which is only a spot.

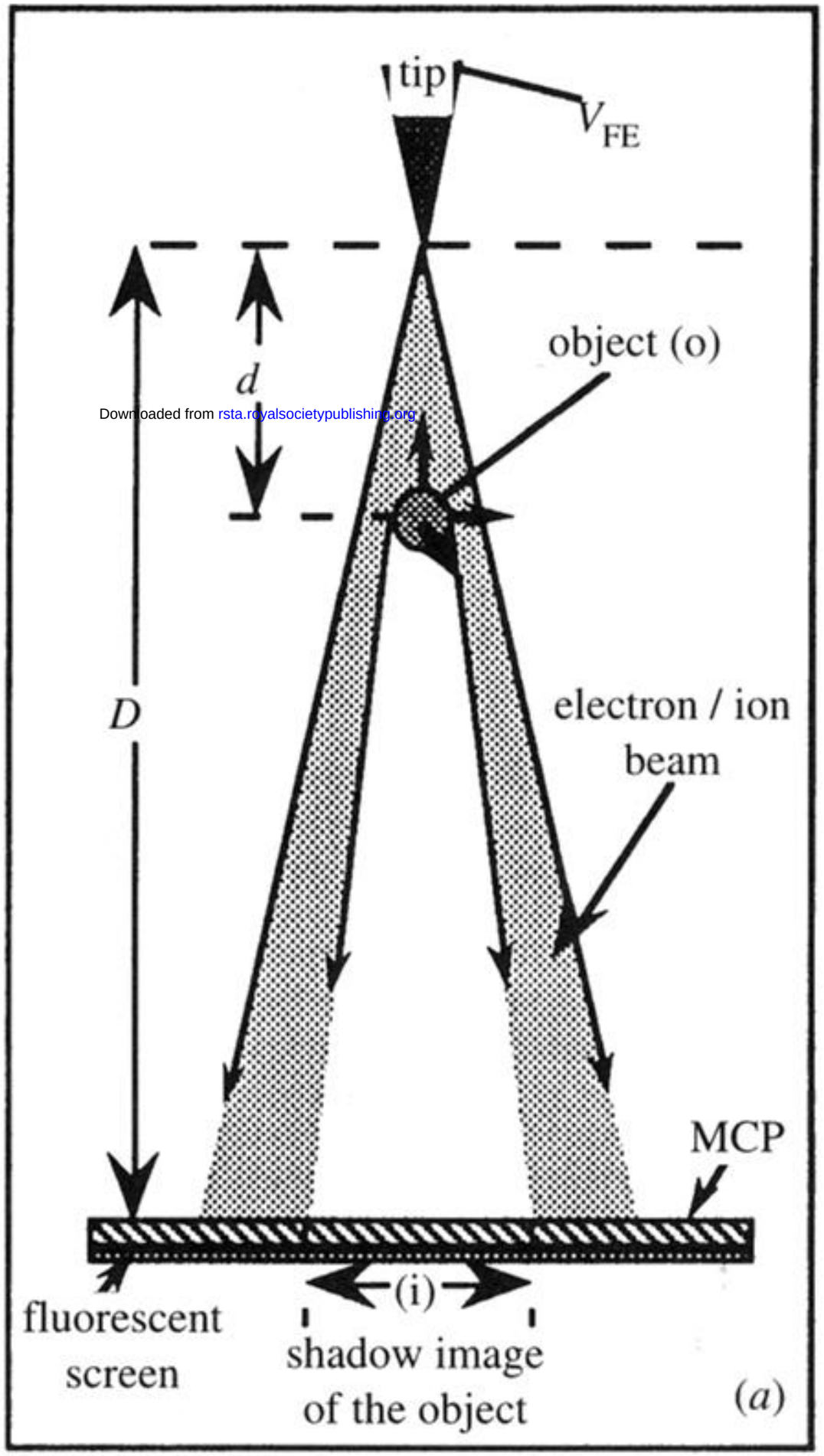

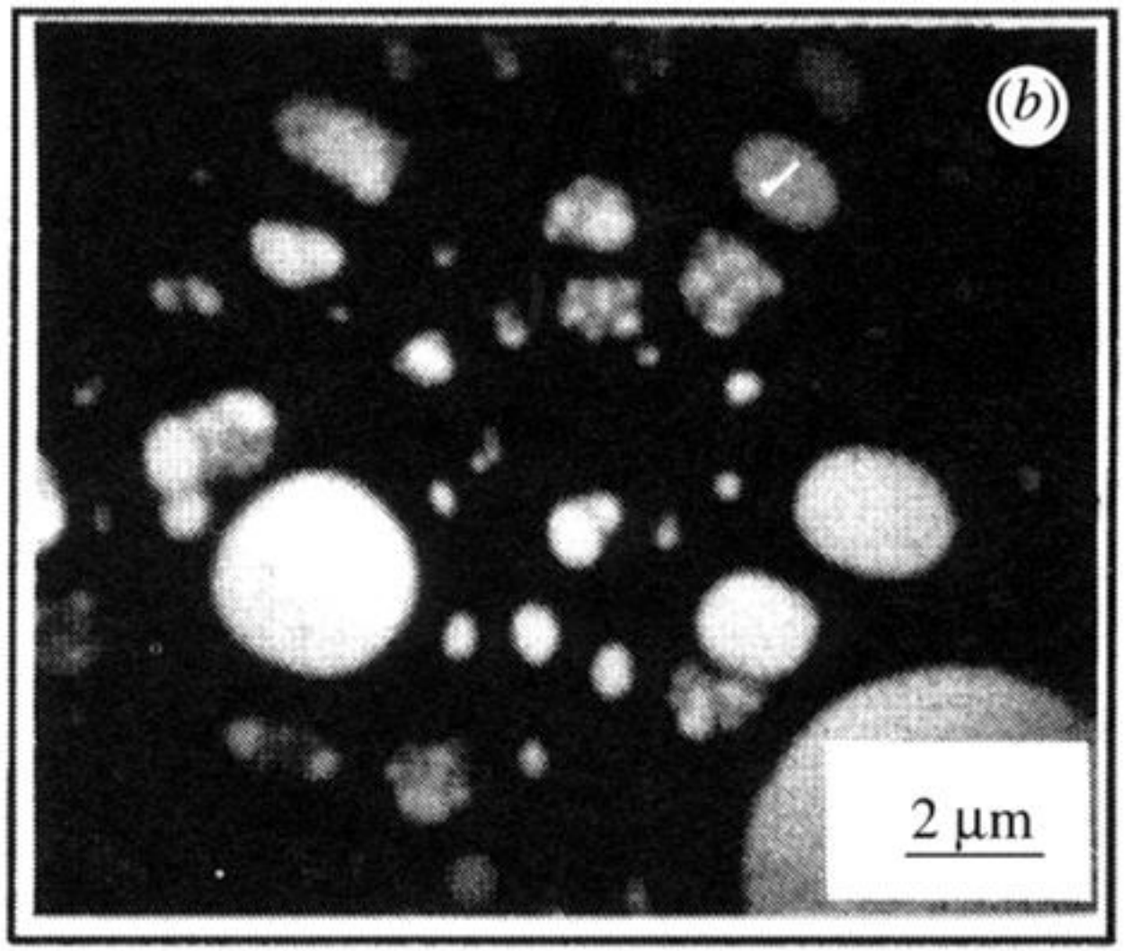

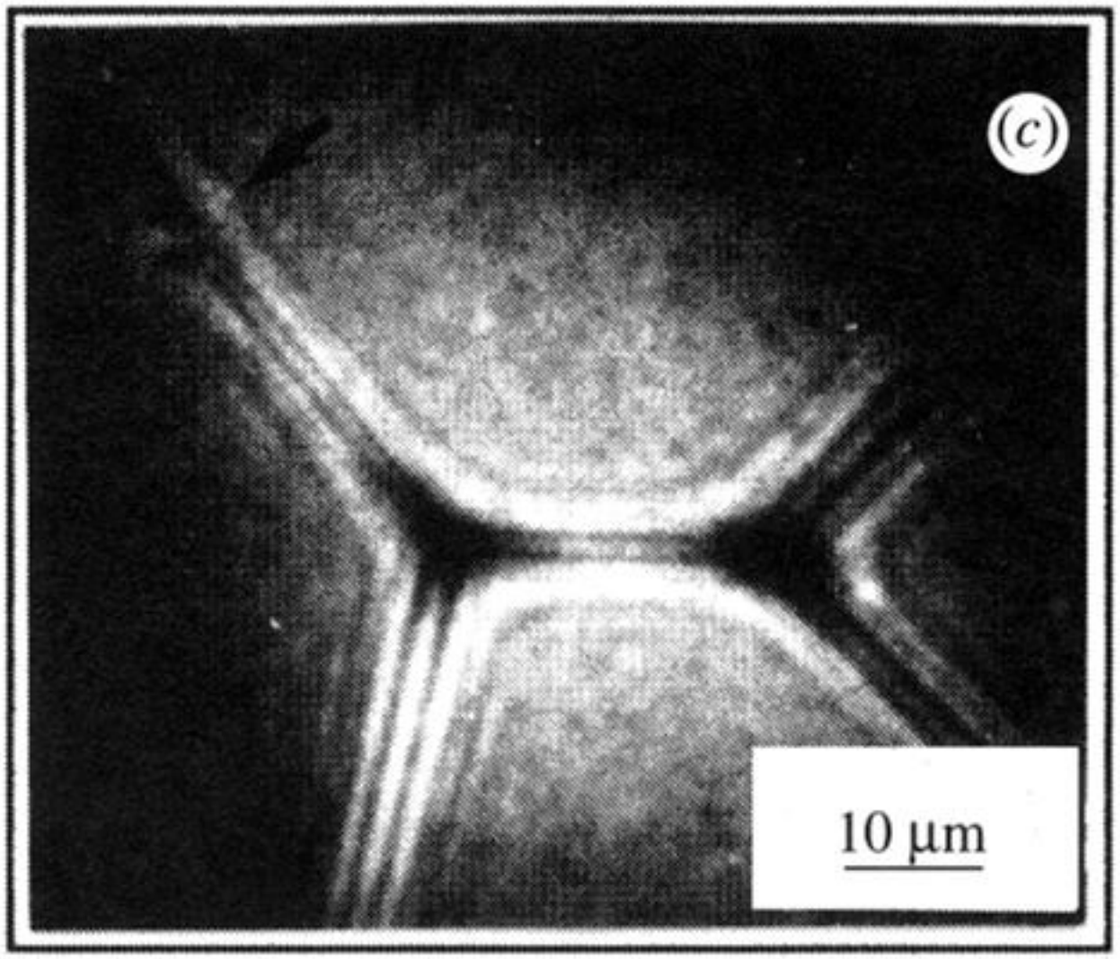

igure 4. (*a*) Schematic drawing of a projection microscope; (*b*) shadow image of carbon holes t low magnification (380 V); (*c*) Fresnel diffraction by carbon fibres (290 V). The arrow shows nanometric defect on the fibre.

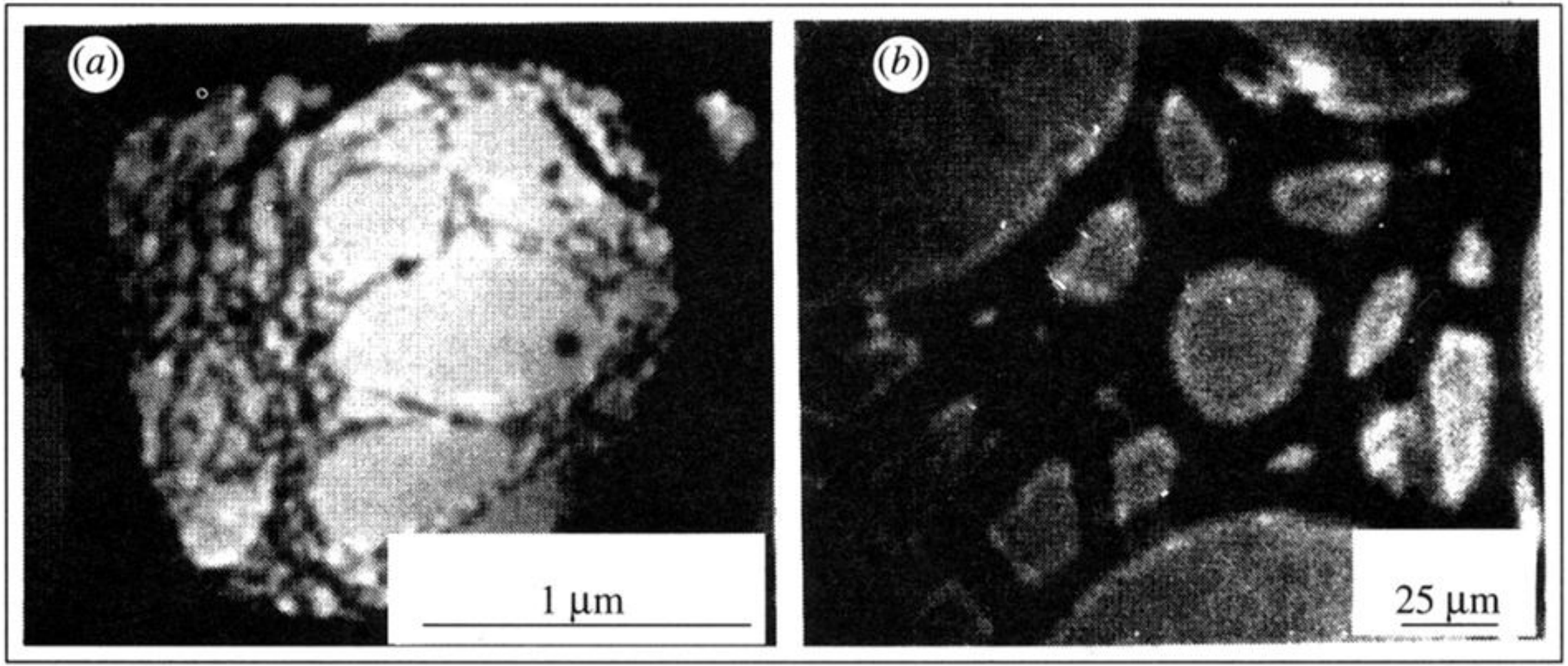

igure 5. Projection microscopy images of polymers stretching across a carbon hole: (*a*) 720 V; (*b*) 270 V.